Integration of the barotropic vorticity equation on a spherical geodesic grid

By DAVID L. WILLIAMSON, *Massachusetts Institute of Technology, Cambridge, Massachusetts,* and *National Center for Atmospheric Research, Boulder, Colorado*

(Manuscript received September 25, 1967; revised version May, 20, 1968)

ABSTRACT

A quasi-homogeneous net of points over a sphere for numerical integration is defined. The grid consists of almost equal-area, equilateral spherical triangles covering the sphere. Finite difference approximations for a nondivergent, barotropic model expressed in terms of a streamfunction are proposed for an arbitrary triangular grid. These differences are applied to the spherical geodesic grid. The model is integrated for 12-day periods using analytic initial conditions of wave number six and four. The numerical solution with these special initial conditions follows the analytic solution quite closely, the only difference being a small phase error. Small truncation errors are noticeable in the square of the streamfunction averaged over latitude bands.

1. Introduction

The advent of today's large, fast computers has made it possible to treat meteorological problems over the entire earth. A fundamental problem which naturally arises is the definition of the points on the sphere at which finite-difference equations are to be applied. Various grid systems over a sphere and accompanying difference schemes have been suggested and tried with varying degrees of success. Kurihara (1965) has summarized many of these.

One grid property which seems to be desirable for some problems but lacking in most grids used to date is homogeneity. For example, in numerical weather prediction, if the fields to be predicted have a uniform scale over the entire earth, then a homogeneous grid seems well suited to the problem. Of course, if the scale in the tropics differs greatly from that, say, in the polar regions, then a homogeneous grid may not be desirable. Kurihara (1965) had defined a homogeneous grid over the sphere. Integrations with a nine-level Model (Kurihara & Holloway, 1967), produced seemingly satisfactory results. Grimmer & Shaw (1967) performed integrations of a free surface model using a similar grid. They found that for initial conditions given by a solution of the nondivergent vorticity equation, the differential phase-truncation error led to a rapid departure from the analytic solution.

Kurihara's grid, although homogeneous, has grid points placed around latitude circles. This feature may lead to spurious results in zonally averaged quantities. In the following we introduce a new homogeneous grid eliminating this feature and present corresponding difference approximations for a nondivergent barotropic model. Results of test integrations are presented.

Many people have noted the similarity between Buckminster Fuller's Geodesic Domes, constructed from plane triangles (see McHale, 1962, for a collection of photographs of such domes), and a sphere. This close similarity leads one to believe a spherical grid can be defined in a similar fashion. A similar division of the globe was used for geomagnetic studies by Vestine *et al.* (1963). The name *spherical geodesic* grid follows from defining the grid as a collection of geodesics, or arcs of great circles.[1]

[1] After this report was prepared, the author learned that similar calculations were performed by Robert Sadourny, Akio Arakawa, and Yale Mintz at the Department of Meteorology, UCLA, and issued as a Numerical Simulation of Weather and Climate Technical Report No. 2 entiled "Integration of the non-divergent barotropic vorticity equation with an icosahedralhexagonal grid for the sphere".

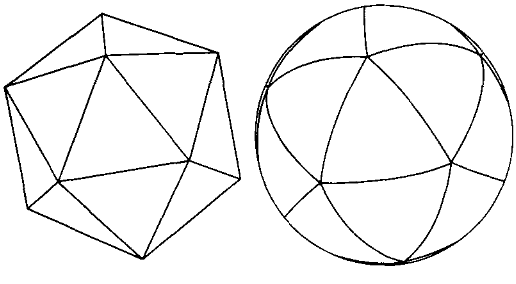

Fig. 1. An icosahedron and an icosahedron expanded onto a sphere.

2. Spherical geodesic grid

The spherical geodesic grid consists of a number of almost, but not quite, equal-area, equilateral spherical triangles covering the entire sphere. There are many methods of defining such a grid. Basic to those considered here is an icosahedron, the geometric solid with 20 equilateral-triangular faces, constructed inside a sphere with its twelve vertices on the sphere. We denote the 20 triangles of the icosahedron as *major triangles*. The vertices of the major triangles can be connected by great circles to form 20 congruent *major spherical triangles* covering the sphere (Fig. 1). These major spherical triangles are then subdivided into smaller *grid triangles*.

One possible grid is defined by dividing the major triangles into smaller congruent triangles and projecting these onto the sphere. Let each side of a major triangle be divided into n equal segments, where $n = 2^m$ for some integer $m \geq 1$. Perpendicular lines are constructed from the division points to the opposite sides, as in Fig. 2. Each major triangle then contains $3n(n-2)/4$ complete congruent equilateral plane triangles, with n half triangles along each edge. The vertices of these smaller triangles are projected onto the surface of the sphere by a ray from its center and connected by great circles to form the spherical grid triangles.

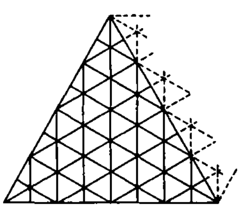

Fig. 2. Division of major plane triangle into smaller congruent triangles ($n = 8$).

A second possible grid, the one used for the integrations presented here, is defined as follows. Examination of an icosahedron shows that it can be separated into five sets of four triangles. For convenience we place the end vertices of each set at the north and south poles as in Fig. 3. (This restriction is easily removed.) With this orientation, the north and south poles are common to all five sets of four triangles.

The sides of the major spherical triangles are now divided into n equal arcs (again $n = 2^m$). In this case, three sets of great circles do not always intersect at one point as straight lines do in the plane case. Hence the two sets shown as solid lines in Fig. 3 are used to define the grid points in ACD. The points are projected across AC to define the points in ACE. The points in the other two triangles of the set are defined in the same manner using the south pole for reference instead of the north. The grid triangles are formed by connecting the points with great circles (solid and broken lines in Fig. 3). Note that again the sides of the major spherical triangles do not coincide with sides of the grid triangles. The latitudes and longitudes of the grid points can be found in a straightforward manner by applying standard formulas of spherical trigonometry (see Appendix I). Once the positions of the grid points are found for this orientation of the grid, any point can be

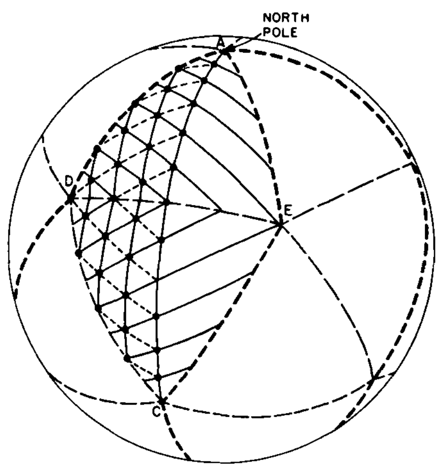

Fig. 3. Division of major spherical triangles into grid triangles ($n = 8$). See text for explanation.

Fig. 4. Spherical geodesic grid with pole at a major triangle vertex.

Fig. 5. Spherical geodesic grid with pole near the center of a major spherical triangle.

made the pole by a simple rotation (Appendix II). Figs. 4 and 5 show the two orientations of the grid used in this study. In Fig. 4 the poles are at vertices of major triangles, and sides of major triangles run in the zonal bands 27 to 33° and −27 to −33°. In the second orientation (Fig. 5), the poles are near the centers of major triangles and there is no narrow zonal band containing sides of major triangles all around the earth.

Each major triangle contains $\frac{3}{2}n(n-2)$ complete grid triangles and each edge bisects n triangles. Therefore the grid consists of $15\,n^2$ triangles. All but 12 grid points are vertices of six triangles, the 12 points are vertices of five triangles. Hence, if N is the number of grid points

$$6 \times (N-12) + 5 \times 12 = 3 \times 15n^2$$

and the number of grid points is given by

$$N = \frac{15}{2}n^2 + 2.$$

We define an average area $\bar{A}$ to be the area a spherical triangle would have if the area of $15\,n^2$ of them equalled the area of the earth, i.e.,

$$\bar{A} = 4\pi r^2/15\,n^2,$$

where r is the radius of the earth. Similarly, a mean grid interval $\bar{h}$ can be defined to be the length of a side of an equilateral triangle having area $\bar{A}$.

$$\bar{h}^2 = 4\bar{A}/\sqrt{3}.$$

Table 1 provides the appropriate values for several values of n taking $r = 6370$ km. We refer to $n = 8$ as a 10° grid and $n = 16$ as a 5° grid. The actual grid interval of the 10° grid varies from 8.59° in the vertices of major triangles

Table 1

n	Number of triangles	Number of grid points	$\bar{A}$ km²	$\bar{h}$ km	$\bar{h}$ Degrees
4	240	122	213×10^4	1911	19.8
8	960	482	53×10^4	1100	9.91
16	3,840	1920	13×10^4	554	4.98
32	15,360	7682	3.3×10^4	276	2.48

to 10.82° in the centers. The grid interval of the 5° grid varies from 4.28° to 5.49°. These grids are therefore not homogeneous in the sense that all grid intervals are equal; however, such triangular grids are impossible to define if the grid interval is less than 63°.

3. Finite difference approximations

As a first test of the spherical geodesic grid, the barotropic model for nondivergent, frictionless flow is used

$$\frac{\partial \zeta}{\partial t} = -J(\psi, \zeta + f), \quad \zeta = \nabla^2 \psi.$$

Here ζ is vorticity, ψ the streamfunction, and f the Coriolis parameter. This model was chosen for the test so that analytic initial conditions with a known solution (Neamtan, 1946), could be prescribed. In doing so, all errors except those due to the numerical methods employed are eliminated.

A finite difference form of the Jacobian or advection term has been proposed by Lorenz[1] for a grid of arbitrary triangules. Consider the polygon, with area A, formed by K triangles surrounding the grid point P_0, such as in Fig. 6 with $K = 5$. The verticies of the polygon are P_1 to P_5. Since the flow is nondivergent, integration of the first equation over this region results in

$$\frac{\partial}{\partial t}\int_A \zeta dA = -\oint_S u_n(\zeta + f) ds,$$

where u_n is the velocity normal to the boundary s. Two approximations are made in applying this equation to the grid. First, the area integral of the vorticity is replaced by $\zeta_0 A$. Second, the absolute vorticity $\zeta^* = \zeta + f$ is assumed to be uniform along each side of the polygon and is given by the arithmetic mean of its values at the end points of the side. Then since $u_n = -\partial\psi/\partial s$, the difference form becomes

$$\frac{\partial \zeta_0}{\partial t} = \frac{1}{2A}\sum_{i=1}^{K} (\zeta_i^* + \zeta_j^*)(\psi_j - \psi_i),$$

where $j \equiv i + 1 \pmod K$.

It is immediately seen that if the total vorticity is defined to be the sum of the vorticity at the grid points weighted by the areas of the surrounding triangles, then total vorticity is conserved. It is also easy to show that kinetic energy and the square of vorticity are conserved.

[1] Private communication, 1966.

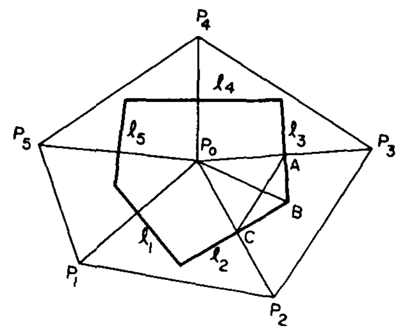

Fig. 6. Grid triangles and points for difference equations.

If this scheme is applied to a rectangular grid by averaging the difference equations obtained from triangulation using either right diagonals or left diagonals, the result is seen to be Arakawa's (1966) scheme. The scheme applied to an equilateral triangular grid on a plane is second order.

As is always the case for models formulated in terms of a streamfunction, it is necessary to solve Poisson's equation. The method used in this test is a sequential relaxation. Thus a difference scheme for the Laplacian is needed. Such schemes have been formulated for triangular grids by MacNeal (1953) and Winslow (1966). We introduce another method. These methods all reduce to the same one for equilateral triangular grids on a plane.

Construct the polygon, with area a, formed by the perpendicular bisectors of the rays P_0P_i of the original polygon (Fig. 6). Integration of $\zeta = \Delta^2\psi$ over a gives

$$\Gamma = \oint_{s'} u_s ds,$$

where Γ is the circulation around the boundary s' of a and u_s is the counterclockwise tangential velocity. Two approximations are used to apply this equation to the grid. First, replace the circulation by $\zeta_0 a$. Second, assume that the tangential velocity $u_s(=\partial\psi/\partial n)$ is constant on each segment of s' and equal to $(\psi_i - \psi_0)/|P_0P_i|$.

The difference approximation is then

$$\zeta_0 = \sum_{i=1}^{K} \omega_i(\psi_i - \psi_0), \tag{2}$$

where $\omega_i \equiv l_i/|P_0P_i|a$ and l_i are the lengths of the line segments of s'.

The solution of Poisson's equation is obtained by a sequential relaxation. The direction of the sweep through the grid is complicated by its being nonrectangular and is not given here. It may be indicated by the usual equations:

$$\left.\begin{aligned} \psi_0^{m+1} &= \psi_0^m + \alpha R^m, \\ R^m &= \frac{1}{\sum_{i=1}^{K}\omega_i}\left\{\sum_{i=1}^{K}\omega_i[\psi_i^j - \psi_0^m] - \zeta_0\right\}. \end{aligned}\right\} \tag{3}$$

j is either m or $m+1$ depending on whether or not the ith surrounding point has been affected by the $m+1$ pass, and α is an overrelaxation coefficient to be determined experimentally.

The forecast can be made by either advancing ζ using $\partial\zeta/\partial t$ or by relaxing for $\partial\psi/\partial t$ from $\partial\zeta/\partial t$ and advancing ψ. The latter method is used here. The initial guess for the relaxation in the first time step is a zero field. The second time step uses the $\partial\psi/\partial t$ field from the first step for the initial guess and the general time step uses an extrapolation from the fields at the two previous times for the first guess. The relaxation is continued until the residue R is less than some prescribed convergence limit ε at all points. See Thompson (1961) for information concerning standard relaxation procedures used in meteorology. Any suitable time stepping may be used. Centered time differences are used in the following integrations with a foreward time step initially.

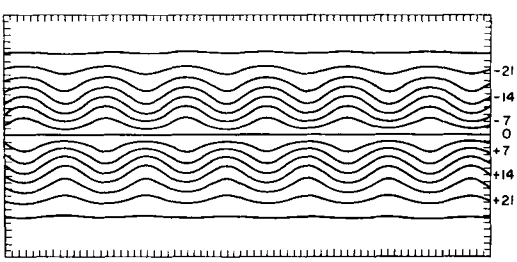

Fig. 7. Initial wave number six ψ field. Intersections of 5° latitude, longitude lines are projected onto a rectangular grid for the figure. The equator has zero ψ value. Contour interval is 3.5×10^7 m² sec⁻¹, negative to north and positive to south.

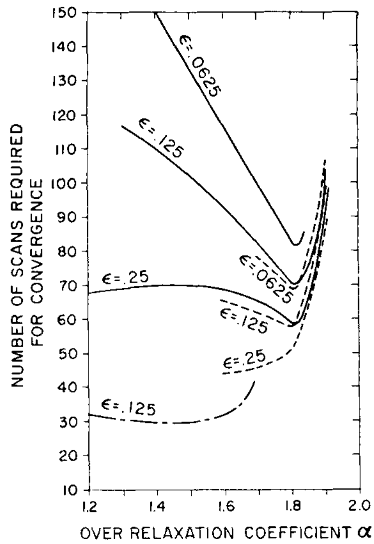

Fig. 8. Convergence speed of relaxation. Dashed lines are for the grid of Fig. 5, solid are for that of Fig. 4. The dash-dot line is a corresponding curve from Gates and Riegel converted to our coordinates.

4. Initial conditions

The nondivergent barotropic model is chosen for the first test of the spherical geodesic grid since it has known solutions in the form of waves travelling around the earth with constant angular velocity and without change of shape. By using such analytic initial conditions we can determine exactly the total error, sum of roundoff and truncation, of the numerical scheme. Since Gates & Riegel (1962) integrated the same model over a sphere, we can use their initial conditions to allow also a direct comparison between the two difference schemes. Their initial and verification fields of ψ are

$$\psi = -279.68 \sin\varphi + 136.65 \sin(6\lambda - \nu t)\sin\varphi\cos^6\varphi, \tag{4}$$

in units of km² sec⁻¹. The pattern moves eastward with angular velocity $\nu/6 = 20°$ long. per day. Fig. 7 shows the field given by (5).

5. Errors in initial time step

As a first step in the error analysis, the model was run for one time step starting at time zero and the errors were examined as a function of

Table 2

ε ...	.25		.125		.0625	
α						
1.6	65.5	−65.5	66.7	−66.9	69.0	−69.1
	69.4	−69.5	66.5	−66.5	—	—
1.7	65.4	−65.2	67.5	−67.8	69.5	−69.7
	67.9	−67.8	65.4	−65.5	64.3	−64.4
1.8	65.7	−66.4	68.9	−69.3	70.6	−70.8
	63.4	−63.8	63.3	−63.5	63.5	−63.5
1.9	71.0	−71.7	71.4	−71.5	—	—
	64.1	−64.9	63.9	−64.3	64.1	−64.1

Maximum positive and negative errors of $\partial\psi/\partial t$(m^2 sec^{-2}) at $t = 0$. The upper numbers are for grid of Fig. 4, the lower ones for grid of Fig. 5.

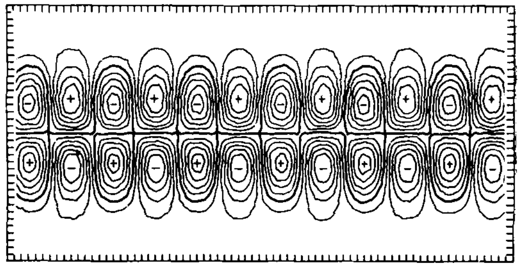

Fig. 10. Exact ζ values at time $t = 0$. The dark line is the zero line; contour interval $= 7 \times 10^{-6}$ sec^{-1}. The figure was produced by the computer using linear interpolation within grid triangles. This causes the small irregularities in this and previous figures.

grid orientation, overrelaxation coefficient and convergence criterion

The speed of the relaxation process for the 5° grid is shown in Fig. 8. The convergence limit $\varepsilon = 0.125$ m^2 sec^{-2} corresponds to approximately 0.07 per cent of the maximum $\partial\psi/\partial t$. One corresponding curve from Gates & Riegel (1962) is given for comparison. The geodesic grid is seen to be more sensitive to variation of overrelaxation parameter than Gates and Riegel's grid. It is also seen to be slower; however, Gates and Riegel's results are for only one hemisphere with fewer points. The second orientation of the grid is systematically faster than the first. This was also observed in similar tests with a 10° grid. The fastest convergence is around $\alpha = 1.8$ for all except one case. Winslow (1966) reports an optimum value between 1.9 and 1.96 for linearized overrelaxation in a nonuniform triangular mesh on a plane. One should remember that the results in Fig. 2 apply only to the first time step with initial conditions (4). The relaxation is considerably faster with the extrapolated first guess. The scheme converges on the average in less than 20 iterations with $\alpha = 1.8$, $\varepsilon = 0.125$, and the grid of Fig. 5.

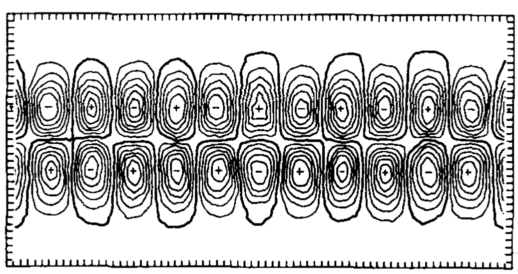

Fig. 9. $\partial\psi/\partial t$ error at time $t = 0$, $\alpha = 1.7$, $\varepsilon = 0.125$, and for grid of Fig. 5. The dark line is the zero line; contour interval is 10 m^2 sec^{-2}.

The error in the computed solution of $\partial\psi/\partial t$ is shown in Fig. 9 for $\alpha = 1.7$, $\varepsilon = 0.125$ and grid of Fig. 5. The error consists of cells of alternating sign around the hemisphere with negative error (computed minus analytic solution) west of the wave trough and positive west of the ridge. The maximum error of each cell is found between latitudes 20° and 25°, the area of maximum vorticity advection. This type of error field produces a systematic underestimate of the true vorticity advection.

Table 2 lists the largest positive and negative errors of $\partial\psi/\partial t$ at time $t = 0$. These values are about 40 per cent larger than the corresponding values from Gates and Riegel's integrations. Also, our results exhibit a larger and less systematic variation. The actual error patterns are all like Fig. 9 for the other values of α and ε tested.

The errors in Table 2 and Fig. 9 are the accumulation of the errors of all the discrete approximations used. It is also of interest to examine the errors of each phase in the computation. We consider first the error in calculating the vorticity. Fig. 10 shows the vorticity field determined analytically. The error pattern from calculating the vorticity from (2) resembles Fig. 10 closely, negative cells of error coinciding with positive cells of vorticity. This implies that the values of ζ calculated by the difference scheme are too small, and the gradient is smaller than it should be. The ζ error is about 2.0 per cent of the true values with grid orientation 1, and 2.4 per cent with grid orientation 2.

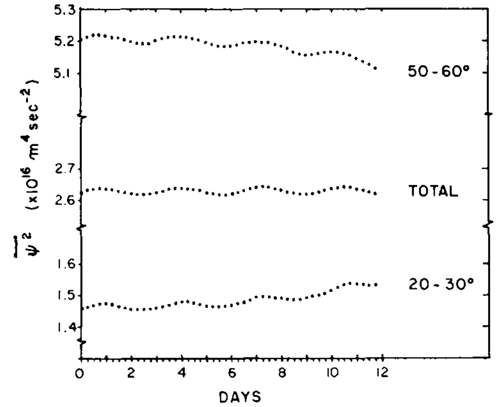

Fig. 11. Variation in ψ^2 averaged over the entire earth and within the latitude bands 20–30° N and 50–60° N, for wave number six.

There is a slight distortion of the error pattern when a zero contour crosses a side of a major triangle.

The pattern of exact values of $\partial\zeta/\partial t$ is like that of Fig. 9, but with uniform cells. The error in the Jacobian approximation using exact values of ψ and ζ also resembles Fig. 9 with positive cells out of phase with those of $\partial\zeta/\partial t$, indicating that the values of $\partial\zeta/\partial t$ are too small. The error in $\partial\zeta/\partial t$ is about 5 per cent. When the values of ζ obtained from (2) are used instead of the exact values, the error is increased to 13 per cent. The error field is also more distorted at sides of major triangles in this case.

The values of $\partial\psi/\partial t$ were found by relaxing the exact $\partial\zeta/\partial t$ field to compare with the values obtained in the previous section. The convergence properties are the same as those with the approximate $\partial\zeta/\partial t$ field. The error using exact $\partial\zeta/\partial t$ values is 50 per cent of that using the approximate $\partial\zeta/\partial t$ values.

6. Twelve day integrations

Initial conditions (4) were integrated for 12 days using 1 hour time steps, $\alpha = 1.8$, $\varepsilon = 0.125$, and the grid shown on Fig. 5. The wave moved eastward without change of shape at a speed of 18.6° per day compared to 20° per day for the analytic solution. No figure showing the final field is included as the only observable difference between it and Fig. 7 would be the phase shift. The wave did not exhibit any tendency for the trough to tilt, as reported by Gates & Riegel (1965), even though the spherical geodesic grid is coarser with respect to the wave at higher latitudes.

Since the analytic solution to these initial conditions is simply a wave moving without change of shape, ψ^2 integrated around latitude bands is constant with time. Other quantities, such as kinetic energy and square vorticity, also have invariant zonal averages for these initial conditions and, of course, invariant global averages for arbitrary initial conditions. Examination of the ψ^2 integrals of the numerical solution furnishes a good check on the accumulation of truncation error in the amplitude of the wave as a function of latitude. Fig. 11 shows a plot of ψ^2 integrated over the entire earth and also over two latitude bands. The middle curve is the average over the entire earth; the upper, for 50 to 60° N, is typical for latitude bands above 40°; and the lower, 20 to 30° N, is typical for latitudes below 40° with little variation near the equator. The averages are obtained by a simple summation of values at the points in a latitude band without weighting the values by the areas represented by the points. The truncation error in this integration is not significant for this wave pattern.

A small oscillation appears in all the averages with a period of about 3.2 days. Since the computed wave moved with speed 18.6° per day, this oscillation can be attributed to truncation error depending on trough position with respect to the grid. To check the hypothesis, the same initial conditions were integrated for 12 days using a 10 degree grid (every other point of Fig. 5) with both one and two hour time steps. In both cases, the wave moved with a speed of 15° per day. The small oscillations again appeared in the averages with a period of 4 days, agreeing with the observed 15° speed.

If these small-scale oscillations are removed from Fig. 11, the mean is seen to increase in lower latitudes, decrease in higher latitudes, and remain steady over the whole globe for the 5° grid. These changes may be a manifestation of truncation error being a function of latitude. Since the wave initial condition is a function of longitude increment, and the grid interval is a function of linear increment, the grid is relatively coarser in high latitudes with respect to the ψ field under consideration.

The integrations using the 10° grid showed the means of all latitude bands increasing with

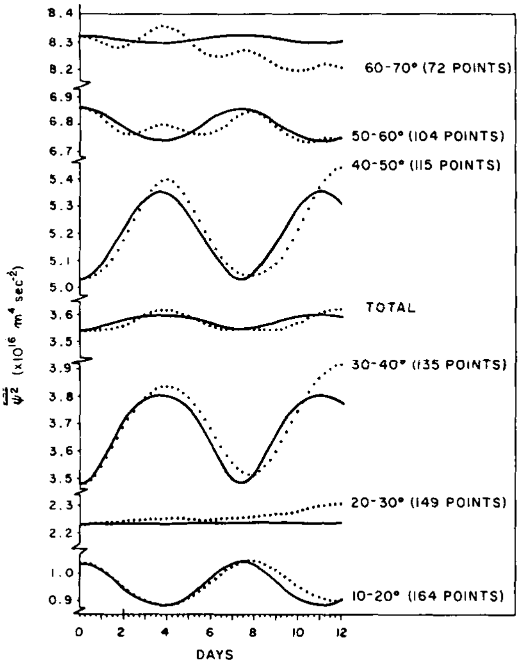

Fig. 12. Variation in ψ^2 averaged in latitude bands and over entire earth. The dotted lines are for numerical integration of wave number four. Solid lines are for analytic values indicating truncation error in the integration over latitude bands as opposed to truncation error in the model itself.

time. The increase was very small for lower latitudes and increased to about 2.5 per cent in 12 days for the higher latitudes above 50°. The global average increased by less than 2 per cent in the 12 days. The resolution of the 10° grid at high latitudes is quite poor with respect to the wave, there being slightly less than four grid triangles per wavelength at 55° and obviously fewer at higher latitudes.

An initial condition of wave number four was also integrated over the 5 degree grid of Fig. 5 using 1 hour time steps. The initial condition is that given by Phillips (1962) as

$$\psi = -318.45 \sin\varphi + 318.45 \cos^4\varphi \sin\varphi \cos 4\lambda, \quad (5)$$

in units of km^2 sec^{-1}. Such a wave moves eastward with a speed of 12.2 degrees per day. Again the actual final pattern after 12 days did not differ significantly from the initial pattern except for the phase shift.

In this case the truncation error in approximating the integration of ψ^2 by an unweighted average over grid points is no longer negligible. Continuous integration of ψ^2 would result in constant zonal averages. However, when the analytic values are summed only at grid points, the result (solid curves in Fig. 12) is seen to vary with a period of about 7.4 days. Such a period corresponds to the pattern moving one wavelength with respect to the grid. The averages of the numerical solution are given as the dotted curves in Fig. 12. The slightly larger period of the numerical solution is caused by the phase truncation error of the scheme. If the truncation error associated with the integration over latitude bands is subtracted, the same comments can be made concerning the truncation error of the model as in the wave number six case.

7. Comments

Some problems involving a relatively thin layer of fluid over a sphere are difficult to solve analytically. Such problems include global-scale atmospheric oscillations, atmospheric general circulation, or even purely fluid dynamical problems such as viscous flow on a sphere. To solve these problems numerically one must use either spectral methods or discrete variable approximations. For the latter method the sphere must be covered by a net of points at which the approximations are applied. If the phenomenon being considered is of uniform scale, it is desirable to use a spatially homogeneous grid for the numerical model. In Section 2 we have introduced such a homogeneous grid and, in the Appendix, a logical map of the grid suitable for computer computations.

The grid is, of course, useless without accompanying discrete approximations to the partial differential equations governing the problem under consideration. We have chosen the nondivergent barotropic model for the first test of the usefulness of the grid. The model approximates large scale atmospheric behavior yet for certain initial conditions has a known analytic solution with which to compare the numerical solution. The difference scheme proposed in Section 3 worked well for this model. The only observable error in the contoured output after 12 days was a small phase error. Examination of the mean square streamfunction revealed small truncation errors in the amplitude, with little accumulation in 12 days.

Of more interest to meteorologists are numerical experiments using primitive models. Work is presently being directed towards formulating finite difference schemes for a primitive barotropic model on a spherical geodesic grid.

Acknowledgements

The author would like to thank Dr. P. Thompson of NCAR and Dr. E. Lorenz of MIT who independently suggested to him the use of such a grid. He would also like to thank Dr. Kasahara of NCAR and Dr. Lorenz for their encouragement during the course of this study. The contour routines for the dd80 visual display unit a NCAR were written by Mr. David Robertson. Bernard O'Lear and Joyce Takamine of NCAR helped with various parts of the code.

The initial portions of the work were performed at MIT under contract No. AF19(628)-5826. The work was completed while the author was a student visitor in the Dynamics Group at NCAR.

APPENDIX I

Locations of grid points

The interior angles of a major spherical triangle are $2\pi/5$ radians. The sides then have length, a, given by

$$\cos \tfrac{1}{2}a = \frac{\cos \pi/5}{\sin 2\pi/5}.$$

By the law of sines, the altitude b is given by

$$\sin b = \sin a \sin 2\pi/5.$$

Define an indexing system (i, j, k) for the grid as follows. Let $k = 1, 2, 3, 4, 5$ denote the five sets of four major triangles. Then let i, j be indices on each set as shown in Fig. A1. Define the north and south poles to be $(1, 1, k)$ and $[(5n+2)/2, (3n+2)/2, k]$ respectively for $k = 1$ to 5. All grid points are at even values of $i+j$. Since each angle of a major triangle is $2\pi/5$ and since each side is divided into N equal arcs, the angle α_i and β_i of Fig. A1 can be found for $i \leq N/2+1$. By symmetry, the angles made by vertical (i = constant) and right diagonal ($i-j$ = constant) arcs with the base ($j = 1$) are known. Once these are known, the triangle ABC can be solved for the vertical side BC. Similarly, the length of arc from any point below $i = j$ in the first triangle to $j = 1$ can be found. The longitude, angle BPC, and colatitude, side PC can then be found by solving triangle PBC, two sides and the included angle being known.

It is useful to calculate some additional in-

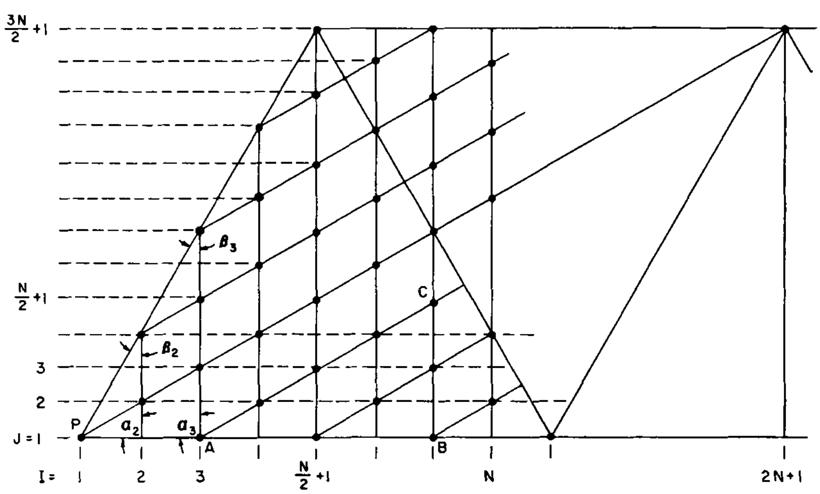

Fig. A1. Logical map of the spherical geodesic grid.

formation once the latitudes and longitudes of points below $i = j$ in the first triangle are known. Solve the triangle shown in Figure A2 for the third side γ_{ij} and the angle Φ_{ij} where $i' = j' = \frac{1}{2}(i+j)$, θ is colatitude, and λ is longitude. This information is used to find the points cf the second triangle.

The location of points below $i = j$ in the second triangle can now be found. Let

$$L = \tfrac{1}{2}(j + 2 - 3(N + 2 - i)),$$

then define $i^* = i - L$, $j^* = j - L$, and $i' = j' = \frac{1}{2}(i^* + j^*)$. Fig. A3 then shows the triangle with two sides and the included angle known which can be solved for colatitude θ and longitude λ.

The points in the first two triangles above $i = j$ are given by reflection across $i = j$. If $i' = i - \frac{1}{2}(i - j)$ and $j' = j + \frac{1}{2}(i - j)$, the colatitude and longitude are given by

$$\theta_{ij} = \theta_{i',j'}, \qquad \lambda_{ij} = 2\pi/5 - \lambda_{i'j'}.$$

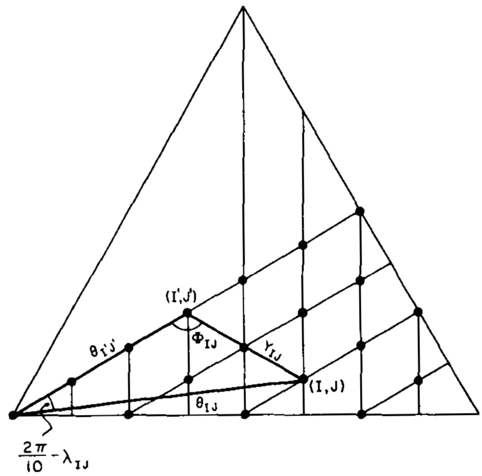

Fig. A2. Logical map of spherical triangles used to find needed arc lengths.

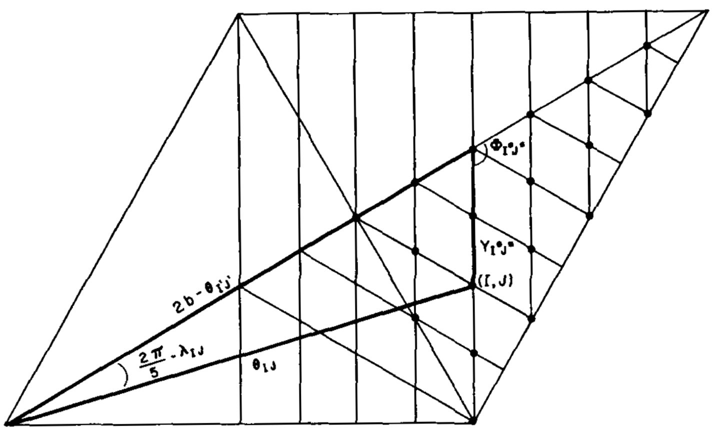

Fig. A3. Logical map of spherical triangles used to find location of grid points in second major triangle

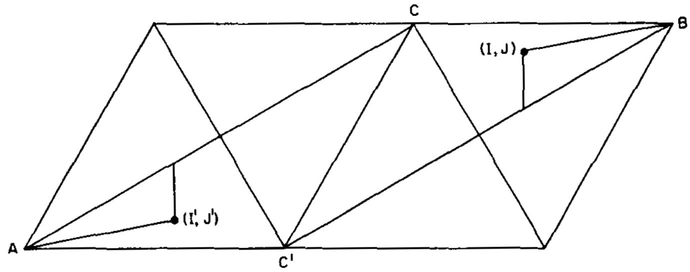

Fig. A4. Logical map of spherical triangles used to find location of grid points in third and fourth major triangles.

The points in the third and fourth triangles can now be easily found. In Fig. A4 note that AC′B is a great circle (0 longitude) and ACB is a great circle ($2\pi/10$ longitude). The figure shows the corresponding triangle used to find the positions in the last two major triangles from those in the first two. Let $i' = 5N/2 + 1 - (i-1)$, and $j' = 3N/2 + 1 - (j-1)$. Then $\theta_{ij} = -\theta_{i'j'}$ and $\lambda_{ij} = 2\pi/10 - \lambda_{i'j'}$.

The above formulas give the position of all points in the first set of triangles, the remaining ones are given by

$$\theta_{ijk} = \theta_{ij}$$

$$\lambda_{ijk} = \frac{2\pi}{5}(k-1) + \lambda_{ij}. \qquad (k = 1 \text{ to } 5)$$

APPENDIX II

Rotation of grid

This section removes the restriction that the point (1, 1, 1) be the north pole. Suppose a point A with colatitude $\alpha < \pi/2$ is to be the pole. Without loss of generality we can assume the longitude of A is π. Define Cartesian coordinates (x, y, z) by

$$z = \sin\varphi,$$
$$y = \sin\lambda\cos\varphi,$$
$$x = \cos\lambda\cos\varphi$$

and a new rotated set (x', y', z') such that $y' = y$ and the z' axis passes through the point A. Then

$$y' = y,$$
$$z' = (\operatorname{sgn} x)[x^2 + z^2]^{\frac{1}{2}} \sin(\operatorname{Arctan} z/x - \alpha),$$
$$x' = (\operatorname{sgn} x)[x^2 + z^2]^{\frac{1}{2}} \cos(\operatorname{Arctan} z/x - \alpha).$$

The corresponding latitude φ' and longitude λ' are then

$$\varphi' = \operatorname{Arcsin} z',$$

$$\lambda' = \operatorname{Arctan}\frac{y'}{x'} + \frac{1 - \operatorname{sgn} x'}{2}\pi.$$

APPENDIX III

Areas of grid triangles

Let A, B, C be three vertices of a grid triangle, and let N be the north pole. The lengths NA, NB, and NC are then the colatitudes of the points A, B, C, respectively. The angles ANB, BNC, and ANC are simply the difference in longitude of the points forming the angle. Thus AB, BC, and CA can be found by the law of cosines. The triangle ABC can then be solved for its angles and the area in terms of the angles.

APPENDIX IV

Weights for the Laplacian

In Fig. 6, the sides P_0C and P_0A are half of P_0P_2 and P_0P_3 respectively, which are given in Appendix III, as is angle $P_2P_0P_3$. Hence, the triangle P_0CA can be solved for side CA and angle P_0AC and P_0CA. Angle BAC is then $\pi/2 - P_0AC$ and angle BCA is $\pi/2 - P_0CA$. Triangle ABC can then be solved for AB and BC, the desired lengths, and the area of P_0CBA can be found.

REFERENCES

Arakawa, A. 1966. Computational design for long-term numerical integration of the equations of atmospheric motion. *Journal of Computational Physics 1*, 119–143.

Gates, W. L. & Riegel, C. A. 1962. A study of numerical errors in the integration of barotropic flow on a spherical grid. *Journal of Geophysical Research 67*, 773–784.

Grimmer, M. & Shaw, D. B. 1967. Energy-preserving integrations of the primitive equations on the sphere. *Quarterly Journal of the Royal Meteorological Society 93*, 337–349.

Kurihara, Y. 1965. Numerical integration of the primitive equations on a spherical grid. *Monthly Weather Review 93*, 399–415.

Kurihara, Y. & Holloway, J. L., Jr. 1967. Numerical integration of a nine-level global primitive equations model formulated by the box method. *Monthly Weather Review 95*, 509–530.
MacNeal, R. H. 1953. An asymmetrical finite difference network. *Quarterly of Applied Math. 11*, 295–310.
McHale, J. 1962. *R. Buckminster Fuller*. New York, George Brazeller, 127 pp.
Neamtan, S. M. 1946. The motion of harmonic waves in the atmosphere. *Journal of Meteorology 3*, 53–56.
Phillips, N. A. 1959. Numerical integration of the primitive equations on the hemisphere. *Monthly Weather Review 87*, 333–345.
Thompson, P. D. 1961. *Numerical Weather Analysis and Prediction*. New York, The Macmillan Company, 170 pp.
Vestine, E. H., Sibley, W. L., Kern, J. W. & Carlstedt, J. L. 1963. Integral and spherical-harmonic analysis of the geomagnetic field for 1955. 0, Part 2. *Journal Geomagnetism and Geoelectricity 15*, 73–89.
Winslow, A. M. 1966. Numerical solution of the quasilinear Poisson equation in a nonuniform triangle mesh. *Journal of Computational Physics 1*, 149–172.

ИНТЕГРИРОВАНИЕ БАРОТРОПНОГО УРАВНЕНИЯ ВИХРЯ НА СФЕРИЧЕСКОЙ ГЕОДЕЗИЧЕСКОЙ СЕТКЕ

Определяется квазиоднородная сетка точек на сфере для численного интегрирования. Сетка состоит из почти равных по площади равносторонних сферических треугольников, покрывающих сферу. Предлагается конечноразностная аппроксимация бездивергентной баротропной модели, выраженной через функцию тока для произвольной треугольной сетки. Эта схема применяется для случая сферической геодезической сетки. Модель интегрируется для 12-суточного периода, причем начальные данные задаются в виде волны с номером шесть и четыре. Численное решение с этими специальными начальными условиями довольно близко к аналитическому решению. Разница проявляется лишь в малой фазовой ошибке. Малые ошибки аппроксимации становятся заметными для квадрата функции тока, осредненной по кругу широты.